

***In vivo* three-dimensional imaging of normal tissue and tumors in the rabbit pleural cavity using endoscopic swept source optical coherence tomography with thoracoscopic guidance**

Tuqiang Xie

University of California Irvine
Beckman Laser Institute
1002 Health Sciences Road East
Irvine, California 92612

Gangjun Liu

University of California Irvine
Beckman Laser Institute
1002 Health Sciences Road East
Irvine, California 92612
and
University of California Irvine
Department of Biomedical Engineering
305 Rockwell Engineering Center
Irvine, California 92697

Kelly Kreuter

University of California Irvine Medical Center
Pulmonary and Critical Care Division
Orange, California 92868

Sari Mahon

University of California Irvine
Beckman Laser Institute
1002 Health Sciences Road East
Irvine, California 92612

Henri Colt

David Mukai

University of California Irvine Medical Center
Pulmonary and Critical Care Division
Orange, California 92868

George M. Peavy

University of California Irvine
Beckman Laser Institute
1002 Health Sciences Road East
Irvine, California 92612

Zhongping Chen

University of California Irvine
Beckman Laser Institute
1002 Health Sciences Road East
Irvine, California 92612
and
University of California Irvine
Department of Biomedical Engineering
305 Rockwell Engineering Center
Irvine, California 92697

Matthew Brenner

University of California Irvine
Beckman Laser Institute
1002 Health Sciences Road East
Irvine, California 92612
and
University of California Irvine Medical Center
Pulmonary and Critical Care Division
Orange, California 92868

Abstract. The purpose of this study was to develop a dynamic tunable focal distance graded-refractive-index lens rod-based high-speed 3-D swept-source (SS) optical coherence tomography (OCT) endoscopic system and demonstrate real-time *in vivo*, high-resolution (10- μm) imaging of pleural-based malignancies in an animal model. The GRIN lens-based 3-D SS OCT system, which images at 39 fps with 512 A-lines per frame, was able to capture images of and detect abnormalities during thoracoscopy in the thoracic cavity, including the pleura, chest wall, pericardium, and the lungs. The abnormalities were confirmed by histological evaluation and compared to OCT findings. The dynamic tunable focal distance range and rapid speed of the probe and SS prototype OCT system enabled this first-reported application of *in vivo* 3-D thoracoscopic imaging of pleural-based malignancies. The imaging probe of the system was found to be easily adaptable to various sites within the thoracic cavity and can be readily adapted to other sites, including rigid airway endoscopic examinations. © 2009 Society of Photo-Optical Instrumentation Engineers. [DOI: 10.1117/1.3275478]

Keywords: optical coherence tomography; thoracoscopy; thoracoscopic imaging; gradient-index lenses; endoscopic imaging; medical and biological imaging; imaging system.

Paper 09238R received Jun. 11, 2009; revised manuscript received Sep. 21, 2009; accepted for publication Nov. 2, 2009; published online Dec. 22, 2009.

1 Introduction

Lung cancer continues to be a leading cause of death worldwide. It is estimated that 1.3 million people die of lung cancer annually.¹ Although the overall five-year survival rate has increased during recent years, it still remains low at ~15%.² The poor prognosis of the disease can be attributed to its aggressive nature and late-stage detection. Because of the rapid progression of the disease, early detection is vital to decreasing its mortality. Current detection methods are limited to low-dose spiral computed tomography (CT), positron emission tomography (PET), magnetic resonance imaging (MRI), and various thoracoscopic techniques.³ Because of the limita-

Address all correspondence to: Tuqiang Xie, Matthew Brenner, or Zhongping Chen, University of California Irvine, Beckman Laser Institute, 1002 Health Sciences Road East, Irvine, California 92612. Tel: 949-824-3924; Fax: 949-824-8413; E-mail: tuqiang.xie@gmail.com, mbrenner@uci.edu, or z2chen@uci.edu

tion of resolution, CT, PET, and MRI often fail to detect early cancer in the lung, chest wall, pericardium, and other sites, causing many patients to miss the opportunity for early treatment and possible survival. As a surface-imaging technique, white-light thoracoscopy is low resolution and cannot provide morphological or structural visualization below the surface, thus making early diagnosis and determination of size, probability of malignant nature, and extent difficult to assess.

Optical coherence tomography (OCT), an emerging technology, is a noninvasive technique that is able to provide cross-sectional images of biological tissue and offers near-histologic images, with a resolution of approximately 2–10 μm , and an image depth of 2–3 mm.^{4,5} The micron-scale resolution allows for *in vivo* investigation and screening for possible tissue abnormalities. OCT uses light reflected from within tissue to generate two-dimensional (2-D), sectional images of the tissue structure in a manner similar to, but with higher resolution than that obtained by ultrasound. OCT probes can be inserted through a conventional bronchoscope or adapted with rigid endoscopic systems for applications such as thoracoscopy. OCT technology can potentially aid conventional airway biopsies by increasing yield and providing better assurance that accurate margins are obtained. Three-dimensional (3-D) OCT imaging has advantages over 2-D imaging for clinical applications, but requires development of systems with more rapid acquisition capabilities, maintenance of lateral resolution, and dynamic focal distance tuning to meet *in vivo* demands.

Although a number of endoscopic OCT systems have been utilized for *in vivo* clinical evaluations, due to limitations of probe size, their lateral resolution is generally around 20 μm and the contrast of probe OCT systems is not maintained at optimal benchtop system equivalence due to coupling efficiency limitations. This is the first study successfully applying an integrated dynamic tunable focusing graded-refractive-index (GRIN) lens rod-based 3-D swept-source (SS) OCT probe system to perform real-time *in vivo* high-resolution imaging of pleural-based malignancies in our animal model.

2 Materials and Methods

2.1 SS 3-D OCT Imaging System

The schematic of the 3-D *in vivo* SS with adjustable working distance GRIN lens rod probe is shown in Fig. 1(a). The probe component of this system has been described in detail in a previous publication.⁶ A broadband wavelength swept laser source (Santec Corporation, Aichi, Japan) at the sweep rate of 20 kHz with 100 nm FWHM bandwidth centered at 1310 nm produces a polarized beam with maximum power of 5 mW. The output power from the laser was split into a reference and sample arm by a 20:80 coupler with 20% power in the reference arm and 80% in the sample arm. The backreflection signal from the reference mirror and backscattering signal from the sample were redirected to a 2×2 coupler by two circulators located in the reference arm and sample arm, respectively. The interference signal after the 2×2 coupler was sent to a balanced amplified photodetector (PDB120C, Thorlabs Inc.). A 100-MS/s 14-bit high-resolution digitizer (NI, PCI-5122) was used to digitize the fringe signal at a sampling speed of 33 MS/s. The SS-OCT system acquires cross-sectional im-

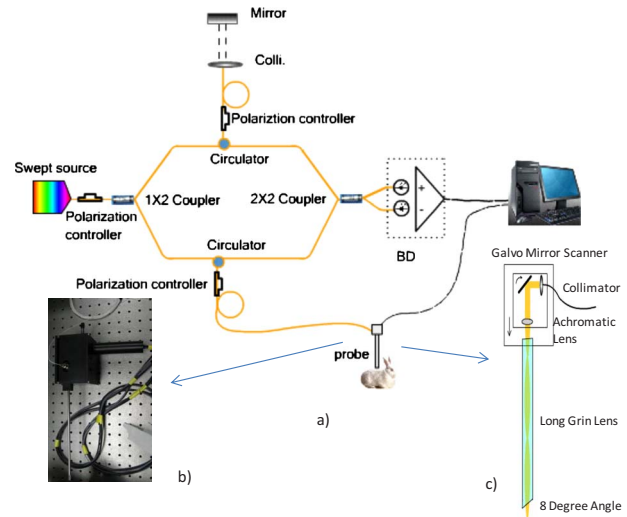


Fig. 1 (a) Diagram of swept source endoscopy OCT system setup and (b) photo of handheld OCT probe.

ages at 39 fps, which are saved in memory and are moved into a hard drive after imaging.

Figures 1(b) and 1(c) shows the photo and schematic of the forward-scanning rigid GRIN lens probe. Sample light from the single fiber was collimated into a beam with a diameter of 4 mm focused by an $f/20$ mm achromatic lens and delivered into the one-pitch GRIN lens (4.58 mm diam, 22 cm length) by a 2-D galvo scanner (6210H, Cambridge Technology Inc., Cambridge, Massachusetts). The distance between the achromatic lens and rod GRIN lens is tunable manually so that probe working distance is tunable within a range of 0–7 mm. Although the probe is located at a fixed position, this dynamic focal distance tuning capability permits the focal point of the sample arm to be adjusted in order to achieve the best image quality during *in vivo* imaging. In the previous design,⁶ the distal end surface of the rod GRIN lens probe caused strong reflections that decreased the system's signal-to-noise ratio (SNR). In order to improve the SNR, a cylindrical glass window with 2 mm thickness and 4.58 mm diam was glued onto the GRIN lens rod, with one surface of the glass window polished to an 8-deg angle relative to the other surface. The surfaces of the wedged glass window and both ends of the GRIN lens rod were coated with a thin antireflective film to further decrease reflections. The long GRIN lens probe caused a dispersion mismatch between the reference and sample arm. This mismatch was measured and compensated for by a software-based numerical method. By use of a mirror as the sample object, the dispersive phase term was measured and averaged from 500 continuous A-lines. The dispersion was cancelled by subtracting the calibrated dispersive phase term from the phase term of the complex depth encoded signal in signal-processing software.^{7,8} The axial and lateral resolutions are approximately 8 and 9 μm , respectively, in our probe OCT system.

In order to illustrate the ability of 3-D OCT images to demonstrate surface topography and subsurface structure of tissues consistent with the gross images as well as histological cross sections of the specimen, 3-D images were constructed. After 512 individual, adjacent, rapid-scanned OCT images

were captured using our probe, they were assembled into a full 3-D image representation of the specimen on line, and these scans were also used to generate a progression of successive individual 2-D OCT images selectively viewed in x , y , or z planes relative to the tissue surface. The system can acquire and display 512 successive individual 2-D OCT images within 13 s. A cylindrical 3-D OCT image with diameter of 4.58 mm can be shown on a monitor in 20 s.

A high-definition digital video endoscopic system was used to scan and thoracoscopically image rabbit chest wall, pericardium, and lung (720 lines, Model No. 222000, Karl Storz, Germany) illuminated with a Xenon (Storz 300, Germany) light source. A 30-deg beveled 4-mm (2.77-mm front objective lens) endoscope with diameter of 4 mm was attached to a digital camera head (Model 7200B, Karl Storz, Germany) and inserted into the thoracic cavity of the rabbit. Tumors in the chest wall were initially located by thoracoscopic examination, and digital video images were recorded. Under guidance by the visual thoracoscopic system, the OCT probe was then used to obtain 2-D cross-sectional and 3-D OCT images of these suspicious lesions.

2.2 Animal Preparation

Male New Zealand white rabbits (Western Oregon Rabbit Supply Company, Philomath, Oregon) weighing 3–4 kg were used in this study under a protocol approved by the Institutional Animal Care and Use Committee. The animals were initially anesthetized with a 2:1 ratio of ketamine HCl (100 mg/ml) (Ketaset, Fort Dodge Animal Health, Fort Dodge, Iowa): xylazine (20 mg/ml) (Phoenix Pharmaceutical, Inc., St. Joseph, Missouri) at a dose of 0.75 cc/kg intramuscularly, in the hind leg. After injection, a 23-gauge 1-in catheter was placed in the animals' marginal ear vein to administer intravenous anesthesia. The depth of anesthesia was evaluated by monitoring the physical reflexes of the animal and pulse rate. Maintenance anesthetic dosed at 0.3 cc of a 1:1 mixture of ketamine:xylazine (ketamine 100 mg/mL: xylazine 20 mg/mL) was administered as needed. A dose of analgesic, Torbutrol 0.1–0.5 mg/kg SQ, was given prior to intubation. The animals were intubated with a 3.0 cuffed endotracheal tube and mechanically ventilated (dual phase control respirator, Model No. 32A4BEPM-5R, Harvard Apparatus, Chicago, Illinois) at a respiration rate of 32/min and a tidal volume of 50 cc and FiO_2 of 100%.

In preparation for the thoracoscopic administration of tumor cells, the right side of the chest was shaved and the rabbit was placed on the operating table with its shaved side up. The operative sites were scrubbed with Nolvasan Surgical Scrub followed by Nolvasan Solution to disinfect the site. The area was then covered with a 40×40 sterile drape.

2.3 Tumor Cell Line

This study used VX2 tumor cells. The cells are classified as carcinomas and are considered to be wholly anaplastic, whose keratinocytes never keratinize.⁹ The tumors are of rabbit origin, known for rapid growth, and have the capability of being transplanted serially. The tumor cell preparation has been described previously.¹⁰

2.4 Tumor Implantation Procedures

A thoracoscope was inserted through the fifth or sixth intercostal space at the midaxillary line using trocars. Under thoracoscopic visualization, a small section of the chest wall parietal pleura was gently abraded with the wooden end of a sterile cotton-tip applicator. This mild abrasion technique was developed to enhance the likelihood of tumor cell adhesion and growth. An inoculum of VX2 tumor cells ($9\text{--}15 \times 10^6$ cell in 0.1–0.5 mL of Hanks buffered saline solution) was injected into the right chest cavity adjacent to the abraded pleural surface using a sterile syringe. Once the surgery was completed, the incisions were sewn with O-silk and Nexaband epidermal glue was placed over the incision site. Before recovering the animals, they were given 0.4 cc of Baytril (22.7 mg enrofloxacin/mL) (Bayer Animal Health, Shawnee Mission, Kansas) as a prophylactic to prevent postsurgical infection.

2.5 Thoracoscopic Surgery for OCT Imaging

At 16 days following inoculation of rabbits with tumor cells, a follow-up thoracoscopy was performed using the procedures described above. If there was sufficient tumor growth at that time, then a decision was made to continue with the imaging of the tumors. Once tumors were located, the thoracoscope was inserted into a predetermined location, at an angle so that OCT imaging could be observed. The GRIN lens of the OCT probe was inserted through a trocar placed in a second small incision.

2.6 Terminal Surgery for Tumor Excision

Once the imaging was complete, the animals were euthanized with 1 cc of Euthasol (350 mg pentobarbital sodium and 50 mg phenytoin sodium, Virbac Animal Health, Fort Worth, Texas) administered through the marginal ear vein, followed by 0.5 cc of heparin flush. Once the animals expired, a median sternotomy was performed to obtain the imaged samples for histologic processing and H&E staining, and for comparison to the OCT images generated. Specific tumor location could be assured by leaving the OCT system in place during the median sternotomy as a guide for sample excision. The imaged area including the tumor was excised from the chest wall or lung, mounted on a small piece of cork, and fixed in 10% formalin. The imaged tumor specimen was then embedded in paraffin, cut into sections of 4- μm thickness, and stained with hematoxylin and eosin by standard methods. Further details of histological processing can be found in our previous publication.¹¹

3 Results

Suspicious lesions observed thoracoscopically in the tumor cell-injected rabbit could be found on the lung, chest wall, pleura, and pericardium approximately 16 days postinjection. Lesions were located by appearance as seen in the chest wall tumor example shown in Fig. 2(a). Because the thoracoscope reveals only surface details, it is sometimes difficult to distinguish normal surface irregularities from tumor and features of the lesion below the surface, including size, borders, and organization, cannot be ascertained. Insertion and guidance of the OCT probe to the site of interest could be accomplished *in*

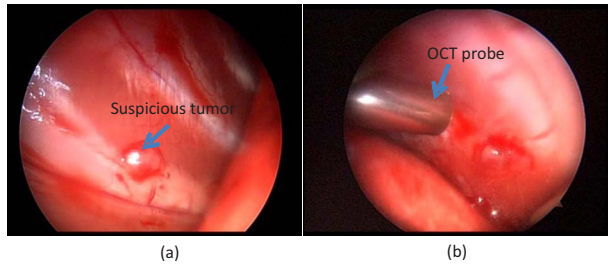


Fig. 2 (a) *In vivo* video endoscope image of suspicious chest wall lesion and (b) the OCT probe acquiring OCT image scans of the lesion.

in vivo in real time through the thoracoscope system as shown in Fig. 2(b). The OCT probe captured 475 individual cross-sectional images that were displayed on the computer monitor in real time. They were assembled into a 3-D volumetric image on site, and this 3-D volumetric image could be orientated to any viewing angle to reveal the full profile of the whole tissue as shown in Figs. 3(a)–3(c). This provides more information to assist in the immediate assessment of abnormal tissue from different viewing angles. The 3-D volumetric image of the chest wall in Figs. 3(a)–3(c) demonstrates a tumor on the chest wall viewed from different angles. This 3-D volumetric image can also be deconstructed in different directions and each section displayed individually to show more detailed information in cross section. Figures 3(d) and 3(e) show the 2-D cross-sectional OCT images deconstructed from a typical 3-D volumetric image. Both cross-sectional images of the chest wall tissue can be used to further evaluate the organizational microstructure of the tissue and differences between the tumor and normal epithelium.

On screening the chest cavity using the thoracoscope, when a suspicious area of possible tumor was observed, the 3-D OCT probe was used to image this area at 39 fps and a total of 495 cross-sectional 2-D OCT images were captured. An *in vivo* reconstructed 3-D OCT volumetric image of a portion of rabbit lung with a tumor is shown in Fig. 4. Figures 4(a)–4(c) show the reconstructed image as viewed at different angles. Three typical 2-D cross-sectional OCT images are shown in Figs. 4(d)–4(f). Figures 4(e) and 4(f) demonstrates the mass and its margins in the lung tissue. The OCT image in Fig. 4(d) demonstrates normal lung tissue from an area adja-

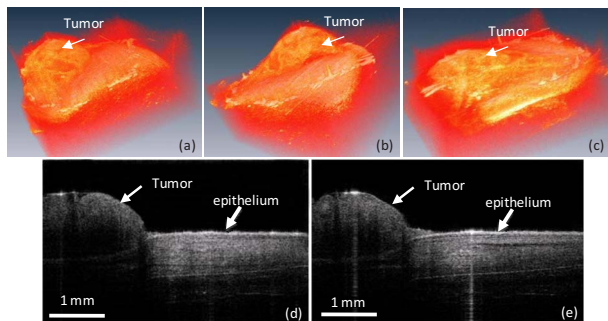


Fig. 3 (a–c) *In vivo* reconstructed 3-D volumetric image of rabbit chest wall with tumor viewed at three different viewing angles and (d, e) 2-D OCT cross-sectional images from within the 3-D volumetric image (a). Image size in (d–f): 4.58 mm (width) by 2 mm (depth).

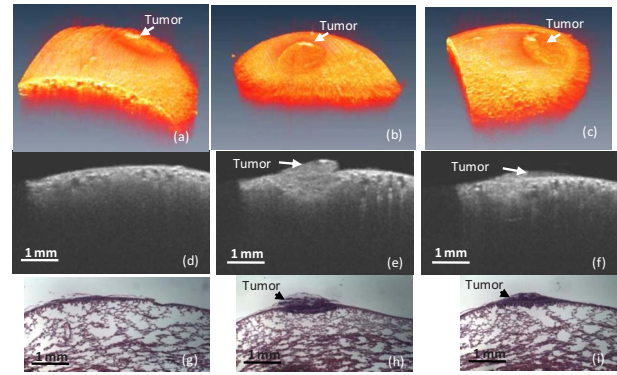


Fig. 4 (a–c) *In vivo* reconstructed 3-D OCT volumetric image of rabbit lung with tumor at different viewing angles and (d–f) 2-D OCT cross-section images from the 3-D volumetric image of and area of normal (d) and abnormal (e, f) lung tissue. Histology of corresponding normal (g) and abnormal (h, i) lung tissue imaged by OCT (a–f). Image size in (d–f): 4.58 mm (width) by 2 mm (depth).

cent to the tumor. These results were confirmed by matching OCT images [Fig. 4(d)–4(f)] to histological sections of the same tissue [Fig. 4(g)–4(i)].

4 Discussion

Thoracoscopic screening of the pleural cavity allows for initial identification of suspicious areas on the chest wall, lung, pleura, and pericardium, and can provide visual guidance for the accurate placement of an OCT probe. Thoracoscopy does not, however, provide detailed histological level resolution assessment of the extent, depth, or subsurface characteristics of lesions. As OCT technology continues to develop, such details could potentially be provided by fast, high-resolution systems that may prove to be extremely valuable in guiding more precise choices regarding choice of biopsy sites.

Since the introduction of time-domain OCT in the early 1990s,^{3,12} OCT has been applied widely to image various biological tissues *ex vivo* and more recently *in vivo*. To our knowledge, this study presents the first report of *in vivo*, fast 3-D thoracoscopic imaging. Compared to time-domain OCT, frequency-domain OCT (spectrometer based or swept source based) has proved to provide higher acquisition speed, which is additionally enhanced at video rates, and better SNR.¹² However, in addition to the increase in imaging speed, miniaturization and maintenance of the high delivered resolution of the OCT probe is critical for *in vivo* 3-D imaging of internal organs or tissue. Numerous OCT endoscopy probe configurations, including those employing microelectromechanical systems (MEMS) mirrors, MEMS rotational motors, fiber bundles, and others have been proposed and implemented specifically for imaging particular organs.^{3,12–14}

OCT has been applied widely in imaging various biological tissues *ex vivo*,^{3,12–19} and different endoscopic OCT systems have been developed for *in vivo* evaluation of various organ systems.^{3,7,20,21} OCT probes can be classified into two types: flexible probes and rigid probes. A flexible probe performs B scans by rotating or moving the whole probe, which mainly consists of an optical fiber, GRIN lens, and prism, or by steering the light beam with a micromotor in the probe.^{6,20,21} Rigid probes can perform B scans using MEMS

mirror technology, which primarily consists of a pigtail GRIN lens, MEMS mirror, and focusing lens, which are packaged in the probe,²² or by a galvo, which is outside of the probe itself and includes a focusing lens and fiber bundle or GRIN lens rod.^{6,23} When the scanner is packaged into the probe, the size of the MEMS actuator or mirror on the MEMS will limit the beam size and the focusing spot, which determines lateral resolution and the receiving efficiency. These degrade the contrast and imaging depth as diameter is reduced. As a result, most endoscopic OCT systems are unable to reach the same resolution and image quality as their benchtop OCT counterparts, which can reach 9 μm of lateral resolution or better if not for the limitation of probe size necessary for access during *in vivo* applications. Our 2-D scanner is mounted in a handheld box and the size of the two scanning mirrors are comparable to benchtop systems and the imaging quality from our endoscopic OCT system is comparable to the benchtop OCT system without compromise because of probe size and the imaging quality due to light collection efficiency. We have previously reported a GRIN lens rod-based probe.⁶ This rigid GRIN lens probe has a diameter of 4.5 mm, and the working distance for the probe is tunable. The probe can be designed to provide either forward- or side-scanning imaging. Because the scanning and focusing hardware are not contained within the rigid probe, this endoscopic OCT can have two larger mirrors driven by 2-D scanning galvo to couple and steer the light beam and additionally, a larger collimator and a focusing lens to assure higher lateral resolution and better coupling efficiency. In comparison to other endoscopic OCT probes, the probe in this study can be minimized to the same small size, and the current design can attain both lateral and axial resolutions of 10 μm with good contrast, equivalent to our benchtop OCT systems. Furthermore, this probe is more durable than probes incorporating MEMS actuators. In addition to the collection efficiency, imaging speed is another factor that affects the image quality, because faster imaging reduces motion artifacts during *in vivo* imaging. Compared to earlier time-domain systems, the SS OCT system without mechanical scanning in the reference arm for each A-scan can increase imaging speed more than 10 times and realize *in vivo* imaging speeds of 39 fps by our probe with 3-D processing in real time. The small size and durability of our probe should make it adaptable to use as an imaging tool for additional clinical applications, including the use of this probe during rigid airway bronchoscopic imaging examination. Probes of multiple pitch lengths can be produced, with the correct length to be determined by the needs of specific applications.

Although most of the reported endoscopic OCT systems provide individual cross-sectional slice images that are representative of the tissue directly under the linear scanning beam, images of an individual cross section does not represent the full 3-D microstructure under the probe. Single scanning may not demonstrate important features of tissue, including those characteristic of pathologic changes. For a more complete understanding of the nature and degree of abnormalities or recognition of tumor and tumor margins within examined tissue, multiple or 3-D OCT images obtained *in vivo* and an overall assessment of the tissue from the evaluation of multiple individual images or 3-D reconstructions would be extremely helpful.

During *in vivo* clinical diagnosis, both the imaging speed

of the OCT itself and the probe scanning speed are critical. Because each OCT probe scan covers only a circular area with a diameter of 4.5 mm, it would be difficult and tedious to scan a large area of tissue with OCT to accomplish initial screening for suspicious lesions *in vivo*. Therefore, while an imaging modality for OCT with much higher speed is required for high-density 3-D imaging, a more effective surface imaging tool is also needed to guide the OCT scanning for *in vivo* imaging. In this paper, we combine a high-speed 3-D OCT endoscope with a thoracoscope to simultaneously image normal tissues and chest wall, lung, and other tumors in a rabbit model of pleural cancer *in vivo*. This combination provides the foundation for development of a future clinical system, which may allow rapid detection and diagnosis of early chest wall, lung, and other pleural cavity cancers.

5 Conclusion

We demonstrate the first *in vivo* thoracoscopic imaging of pleural cancer using a 3-D swept source OCT system utilizing an improved forward-scanning rigid GRIN lens rod probe. Real-time *in vivo* imaging as fast as 39 fps (512 A-lines per frame) is realized. Unlike most other endoscopic OCT systems reported, both lateral resolution and SNR in this endoscopic OCT system are equivalent to our benchtop system without degradation. *In vivo* 3-D imaging of the rabbit chest wall and lung was demonstrated, and not only could the tissue microstructure be delineated, but rotating 3-D images can be displayed at different viewing angles on site. The normal tissue and tumors on the chest wall can be differentiated *in vivo* by 3-D imaging that includes both surface morphology and internal tomography.

The dynamic tunable focusing range and rapid speed of this probe and SS prototype system enable near histologic resolution imaging of pleural-based malignancies. The imaging probe of the system was found to be easily adaptable to various sites within the thoracic cavity. The dynamic focusing range and ability to rapidly capture images, along with the static design of the probe, make it potentially an ideal diagnostic tool for pleural and other *in vivo* rigid endoscopic clinical diagnostic applications.

Acknowledgments

The authors thank Tanya Burney for technical support, and Leaky Liaw and Linda Li for histological preparations reported in these studies. This research was supported by NIH R01 Grant No. CA124967, NIH EB-00293, EB-10090, a-91717, RR-01192, Air Force Office of Scientific Research FA-9550-04-0101, and the Beckman Laser Institute..

References

1. M. Ezzati and A. D. Lopez, "Estimates of global mortality attributable to smoking in 2000," *Lancet* **362**, 847–852 (2003).
2. J. R. Jett, "Limitations of screening for lung cancer with low-dose spiral computed tomography," *Clin. Cancer Res.* **11**(13 Pt 2), 4988s–4992s (2005).
3. S. C. Whiteman, Y. Yang, D. Gey van Pittus, M. Stephens, J. Parmer, and M. A. Spiteri, "Optical coherence tomography: real-time imaging of bronchial airways microstructure and detection of inflammatory/neoplastic morphologic changes," *Clin. Cancer Res.* **12**(3 Pt 1), 813–818 (2006).
4. H. D. Huang, E. A. Swanson, C. P. Lin, J. S. Schuman, W. G. Sinson, W. Chang, M. R. Hee, T. Flotte, K. Gregory, C. A. Puliafito, and J. G.

- Fujimoto, "Optical coherence tomography," *Science* **254**, 1178–1181 (1991).
5. E. El-Bayoumi and G. A. Silvestri, "Bronchoscopy for the diagnosis and staging of lung cancer," *Semin. Resp. Crit. Care Med.* **29**, 261–270 (2008).
 6. T. Xie, S. Guo, Z. Chen, D. Mukai, and M. Brenner, "GRIN lens rod based probe for endoscopic spectral domain optical coherence tomography with fast dynamic focus tracking," *Opt. Express* **14**(8), 3238–3245 (2006).
 7. M. Brenner, K. Kreuter, J. Ju, S. Mahon, L. Tseng, D. Mukai, T. Burney, S. Guo, J. Su, A. Tran, A. Batchinsky, L. C. Cancio, N. Narula, and Z. Chen, "In vivo optical coherence tomography detection of differences in regional large airway smoke inhalation induced injury in a rabbit model," *J. Biomed. Opt.* **13**, 034001 (2008).
 8. B. Cense, N. Nassif, T. Chen, M. Pierce, S.-H. Yun, B. Park, B. Bouma, G. Tearney, and J. de Boer, "Ultrahigh-resolution high-speed retinal imaging using spectral-domain optical coherence tomography," *Opt. Express* **12**, 2435–2447 (2004).
 9. E. Georges, F. Breitburd, N. Jibard, and G. Orth, "Two Shope papillomavirus-associated VX2 carcinoma cell lines with different levels of keratinocyte differentiation and transplantability," *J. Virol.* **55**(1), 246–250 (1985).
 10. K. A. Kreuter, N. El-Abaddi, A. Shbeeb, L. Tseng, S. Brenner Mahon, N. Narula, T. Burney, H. Colt, and M. Brenner, "Development of a rabbit pleural cancer model by using VX2 tumors," *Compar. Med.* **58**, 287–293 (2008).
 11. T. Xie, S. Guo, J. Zhang, Z. Chen, and G. M. Peavy, "Determination of characteristic of degenerative joint diseases using optical coherence tomography and polarization sensitive optical coherence tomography," *Lasers Surg. Med.* **38**, 852–865 (2006).
 12. H. O. Coxson, B. Quiney, D. D. Sin, L. Xing, A. M. McWilliams, J. R. Mayo, and S. Lam, "Airway wall thickness assessed using computed tomography and optical coherence tomography," *Am. J. Respir. Crit. Care Med.* **177**, 1201–1206 (2008).
 13. A. Popp, M. Wendel, L. Knels, T. Koch, and E. Koch, "Imaging of the three-dimensional alveolar structure and the alveolar mechanics of a ventilated and perfused isolated rabbit lung with Fourier domain optical coherence tomography," *J. Biomed. Opt.* **11**, 014015 (2006).
 14. M. Tsuboi, A. Hayashi, N. Ikeda, H. Honda, Y. Kato, S. Ichinose, and H. Kato, "Optical coherence tomography in the diagnosis of bronchial lesions," *Lung Cancer* **49**, 387–394 (2005).
 15. N. Hanna, D. Saltzman, D. Mukai, Z. Chen, S. Sasse, J. Milliken, S. Guo, W. Jung, H. Colt, and M. Brenner, "Two-dimensional and 3-dimensional optical coherence tomographic imaging of the airway, lung, and pleura," *J. Thorac. Cardiovasc. Surg.* **129**, 615–622 (2005).
 16. Y. Yang, S. Whiteman, D. Gey van Pittius, Y. He, R. K. Wang, and M. A. Spiteri, "Use of optical coherence tomography in delineating airways microstructure: comparison of OCT images to histopathological sections," *Phys. Med. Biol.* **49**, 1247–1255 (2004).
 17. G. Sutedja, "New techniques for early detection of lung cancer," *Eur. Respir. J.* **39**, 57s–66s (2003).
 18. Y. Yang, J. Sule-Suso, A. J. El Haj, P. R. Hoban, and R. Wang, "Monitoring of lung tumour cell growth in artificial membranes," *Biosens. Bioelectron.* **20**, 442–447 (2004).
 19. S. Lam, B. Standish, C. Baldwin, A. McWilliams, J. leRiche, A. Gazdar, A. I. Vitkin, V. Yang, N. Ikeda, and C. MacAulay, "In vivo optical coherence tomography imaging of preinvasive bronchial lesions," *Clin. Cancer Res.* **14**, 2006–2011 (2008).
 20. G. J. Tearney, M. E. Brezinski, B. E. Bouma, S. A. Boppart, C. Pitris, J. F. Southern, and J. G. Fujimoto, "In vivo endoscopic optical biopsy with optical coherence tomography," *Science* **276**, 2037–2039 (1997).
 21. J. Su, J. Zhang, L. Yu, and Z. Chen, "In vivo three-dimensional microelectromechanical endoscopic swept source optical coherence tomography," *Opt. Express* **15**(16), 10390–10396 (2007).
 22. T. Xie, H. Xie, G. Fedder, and Y. Pan, "Endoscopic optical coherence tomography with a modified microelectromechanical systems mirror for detection of bladder cancers," *Appl. Opt.* **42**, 6422–6426 (2003).
 23. T. Xie, D. Mukai, S. Guo, M. Brenner, and Z. Chen, "Fiber optic bundle based optical tomography," *Opt. Lett.* **30**, 1803–1805 (2005).